AFRL-RW-EG-TR-2011-052

THREE-DIMENSIONAL DYNAMIC LOADING OF SAND

J. P. BORG

Marquette University, Dept of Mechanical Engineering
1515 W. Wisconsin Blvd
Milwaukee, WI 53233

L. C. Chhabildas

Air Force Research Laboratory, Munitions Directorate
101 West Eglin Blvd, Suite 135
Eglin AFB, FL 32542

Contract No. FA8651-09-1-0011

February 2011

FINAL REPORT

AIR FORCE RESEARCH LABORATORY
MUNITIONS DIRECTORATE

■ **Air Force Materiel Command** ■ **United States Air Force** ■ **Eglin Air Force Base, FL 32542**

NOTICE AND SIGNATURE PAGE

Using Government drawings, specifications, or other data included in this document for any purpose other than Government procurement does not in any way obligate the U.S. Government. The fact that the Government formulated or supplied the drawings, specifications, or other data does not license the holder or any other person or corporation; or convey any rights or permission to manufacture, use, or sell any patented invention that may relate to them.

Qualified requestors may obtain copies of this report from the Defense Technical Information Center (DTIC) <http://www.dtic.mil/dtic/index.html>.
.

AFRL-RW-EG-TR-2011-052 HAS BEEN REVIEWED AND IS APPROVED FOR PUBLICATION IN ACCORDANCE WITH ASSIGNED DISTRIBUTION STATEMENT.

FOR THE DIRECTOR:

//ORIGINAL SIGNED//
HOWARD G. WHITE, DR-IV
Technical Advisor, AFRL/RWM

//ORIGINAL SIGNED//
LALIT C. CHHABILDAS, ST
Program Manager, AFRL/RW

//ORIGINAL SIGNED//
MATTHEW J. MATYAC, DR-III
Technical Advisor, AFRL/RWMW

This report is published in the interest of scientific and technical information exchange, and its publication does not constitute the Government's approval or disapproval of its ideas or findings.

REPORT DOCUMENTATION PAGE

Form Approved
OMB No. 0704-0188

1. REPORT DATE	2. REPORT TYPE	3. DATES COVERED *(From - To)*
Feb 2011	Final	May, 2009 - Feb, 2011

4. TITLE AND SUBTITLE

Three-Dimensional Dynamic Loading of Sand

5a. CONTRACT NUMBER
FA8651-09-1-0011

5b. GRANT NUMBER

5c. PROGRAM ELEMENT NUMBER
61120F

6. AUTHOR(S)
J.P. Borg
L.C. Chhabildas

5d. PROJECT NUMBER
2303

5e. TASK NUMBER
DW

5f. WORK UNIT NUMBER
97

7. PERFORMING ORGANIZATION NAMES AND ADDRESSES
Marquette University, Dept of Mechanical Engineering
1515 W. Wisconsin Blvd
Milwaukee, WI 53233
Air Force Research Laboratory, Munitions Directorate
101 W. Eglin Blvd, Suite 135
Eglin AFB, FL 32542

8. PERFORMING ORGANIZATION REPORT NUMBER

9. SPONSORING / MONITORING AGENCY NAME(S) AND ADDRESS(ES)
Air Force Research Laboratory, Munitions Directorate
AFRL/RW
101 West Eglin Boulevard
Eglin AFB, FL 32542-6810

10. SPONSOR/MONITOR'S ACRONYM(S)
AFRL-RW-EG

11. SPONSOR/MONITOR'S REPORT NUMBER(S)
AFRL-RW-EG-TR-2011-052

12. DISTRIBUTION / AVAILABILITY STATEMENT
DISTRIBUTION A: Approved for public release; distribution unlimited. Approval Confirmation #AAC/PA 96 ABW-2009-0334, dated 4 August, 2009.

13. SUPPLEMENTARY NOTES

14. ABSTRACT

The objective of this work was to assess the ability of Eulerian hydrocode simulations to model the rapid compaction of loose dry granular sand at moderate strain-rates on the order of 10^3 s^{-1}. The simulated results are compared to data obtained from Hopkinson bar experiments. Simulations were conducted in two configurations: three-dimensional mesoscale simulations and one-dimensional continuum simulations with the inclusion of a porosity model. The goal of the simulations was not to reproduce the experimental results by adjusting material or model properties but rather determine a baseline mesoscale solution given bulk material properties of quartz. An additional goal was to probe the parameter space to determine what physical mechanisms are most essential to reproducing experimental data. It was found that even at these relatively low strain rates, the dynamic yield strength of the underlying material (quartz) had to be increased above the static strength yield strength of 40 MPa. In addition the inclusion of grain-on-grain stiction (friction) plays a major role in the compaction of sand at low strain rates.

15. SUBJECT TERMS
Eulerian hydrocode, granular sand, dynamic loading

16. SECURITY CLASSIFICATION OF: UNCLASSIFIED			17. LIMITATION OF ABSTRACT	18. NUMBER OF PAGES	19a. NAME OF RESPONSIBLE PERSON
a. REPORT	b. ABSTRACT	c. THIS PAGE			1Lt Christopher Vineski
UNCLASSIFIED	UNCLASSIFIED	UNCLASSIFIED	SAR	17	19b. TELEPHONE NUMBER *(include area code)* 850-882-1812

Table of Contents:

List of Figures:

List of Tables:

Introduction

The dynamic compaction of loose dry granular material is fundamentally a multi-scale problem. Many engineering problems involving rapid loading conditions exist at the bulk scale, and examples include planetary impact and crater formation, tectonic plate movement, ballistic impact and penetration events. On a bulk scale, which includes thousands of grains of sand, the material behaves somewhat like a homogeneous hydrodynamic continuum. However as the characteristic dimension of the analysis is reduced, the dominant phenomenological behavior is altered. At smaller scales, on the order to tens of grains of sand, the material forms heterogeneous structure, such as stress bridging, which serves to distribute loads. The result is a complicated stress field where grains within a bridge network carry nearly all of the load and grains outside of a bridge network carry nearly no load. At yet smaller scale, on the order of the grain contact surface, the material contact tensor determines the transmittal of stress from one grain to the next. At even smaller scale (those less than the grain itself) the non-isotropic material rheology behavior, such as grain yield and deformation, plasticity and twinning, establish the dominant phenomenological behavior characteristics. Phenomenology at all of these scales feeds back to the bulk scale and ultimately dictates the response of the overall bulk system. However it remains unclear as to which mechanisms dominate and which, if any, might therefore be neglected. The simulations presented here resolve the dynamic compaction behavior from the bulk scale (although not relative to most engineering systems) to the grain, but not sub-grain. At the scale of the grain and smaller the material is treated as a homogenous continuum solid. Thus the term *meso* scale, which means middle scale, is used to describe the simulations presented here.

In addition to dynamics at multiple scales, the variability associated with loading rate can affect the dynamic response of materials. Quartz has famously demonstrated a rich variety of behaviors as a result of shock loading, including phase transitions, material property variability as a function of driving pressure and sample thickness, as well as stress relaxation effects [i-iv]. The strain rates under investigation here ($<10^3$ s^{-1}) are modest compared to shock loading (10^5~10^6 s^{-1}) but clearly in the dynamic regime. These loading rates are more characteristic of conditions found further way from an impact event, where the bulk material does not necessarily experience uniform loading in excess of the Hugoniot elastic limit (HEL). An example of such a loading condition is a transmitted stress wave emanating from a land mine explosion. The analysis is complicated by the heterogeneous nature of the material and therefore the loading. Although the bulk stress state of the sand does not exceed the HEL, this does not imply that individual grains won't exceed the HEL. The response of heterogeneous systems when subjected to these intermediate strain rates remains of fundamental importance in completing our understanding of the dynamic behavior of sand.

Thus, our aim is to explore the dynamic compaction of a heterogeneous system using a mesoscale numeric approach at low to moderate strain rates. Ultimately it is hoped that these mesoscale simulations can be used to augment experimentation by exploring the state space of a heterogeneous system were experimental measurements are difficult or impossible, and serve as a platform by which continuum models can be developed or refined.

Background

Due to the computational expense associated with resolving a mesoscale simulation, the usefulness as applied to large scale engineering systems remains limited. Thus the need for continuum modeling persists. The variation in material properties associated with heterogeneous systems, the inclusion of void space and void collapse, coupled with the lack of adequate experimental techniques to probe the heterogeneous state, make continuum modeling challenging. Usually, granular materials are modeled as a continuum (i.e. the grains and porosity are treated as a new single material) and are assigned average properties. In so doing the heterogeneous nature of the material and the grain interactions are lost. In these continuum approaches additional constitutive relations such as the sphere collapse models [v], snowplow [vi], P-α [ϖιι], P-λ [ϖιιι] or Σ-alpha [ix] models are used to govern the removal of porosity.

Developments in computer architecture and sophistication in parallelization have allowed large-scale simulations to explore multi scale phenomena. A host of researchers, utilizing a variety of numeric formulations such as Eulerian hydrocodes, finite element or discrete element methods, have successfully used mesoscale simulations to model many types of high rate dynamic phenomena involving heterogeneous materials, including the shock compaction of elemental metals and alloys, the behavior of energetic materials, ceramic alloys and earth materials such as sand [x,xi,xii]. These studies have demonstrated that mesoscale simulations can be used to successfully describe the high rate compaction dynamics without the use of additional constitutive relations, thus corroborating predictions from various analytic porous collapse models and experimental observations [xiii,xiv,xv]. In most of these studies the focus was to numerically predict the bulk material behavior at high strain rates, i.e. Hugoniot behavior. It was shown that simple formulations and simple descriptions on a grain level can combine to resolve complicated dynamics observed on the bulk scale such as the formation of dynamic force chains, void collapse, turbulent like behavior and hot spot formation. This study differs from these in that we aim to explore the dynamic compaction at much lower strain rates, near 10^3 s^{-1}.

Experimental Data

The experimental data, which is compared to the simulations presented here, was obtained from a split-Hopkinson pressure bar [xvi-xix]. The material used in these experimental investigations was silica based, kiln dried fine grain sand. The particle size distribution was between 200-450 μm. The dynamic compressive response of the sand was investigated at various moisture contents ranging from 3% to 20% by weight with all specimens having a dry density of 1.50 g/cm^3. The specimens were confined using a hardened 4340 steel tube with an outer diameter of 25.4 mm, inner diameter of 19.1 mm and length of 50.8 mm. The steel tube is used to achieve high confinement pressures and to replicate a uni-axial strain condition. The incident bar was

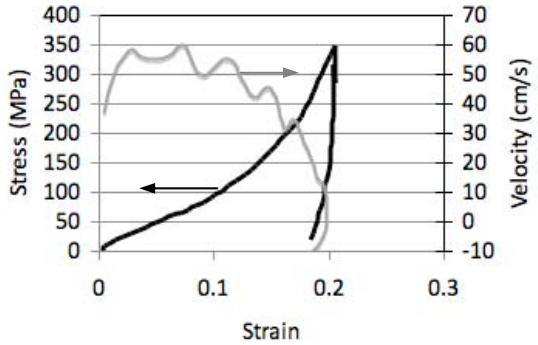

Figure 1: Uni-axial stress-strain behavior of sand, as well as the incident bar velocity, obtained from a split Hopkinson bar at a strain rate of 606 s-1 [16-18].

well controlled in order to produce a near linear strain (constant strain-rate of approximately 600 s^{-1}) over the test interval of 0.2 milliseconds. A representative example of the resulting axial stress data is presented in Figure 1 as a function of strain. The reduction in stress at a strain of approximately 0.2 represents significant unloading of the sample. The strain profile was differentiated in order to produce an incident bar velocity profile, also illustrated in Fig. 1. This velocity profile was used as a boundary condition for the simulations presented below.

Numeric Simulations

The simulations presented here were performed using the CTH hydrocode [xx]. The sand was modeled either as a collection of quartz spheres in a three-dimensional rectilinear domain for the mesoscale simulations or as a single representative material in a one-dimensional domain for the continuum simulations. This was done so that the performance of each type of simulation could be assessed and compared. For both types of simulations, the motion of a rigid driver plate representing the incident bar was prescribed on the left side of the domain and a symmetry boundary condition was imposed on the right side of the domain to represent the longitudinal center of the sample. Figure 1 presents the velocity versus strain history that was used to prescribe the motion of the incident bar for these simulations. For the three-dimensional simulations, periodic boundary conditions were imposed in the lateral direction. Greater detail regarding each type of simulation is presented below.

One-Dimensional Continuum Calculations

Of fundamental importance when conducting continuum simulations of heterogeneous materials is selecting the right constitutive relations; in this work several were investigated, however only one is presented here: a tabular EOS (sesame table) with a P-α compaction model [vii,xxi,xxii]. This equation of state had been previously developed for simulations of buried land mine explosions. The amplitude and duration of transmitted stress waves from land mine explosions is similar to the loading conditions applied by the split Hopkinson bar. A suite of sesame tables for varying soil moisture content has been included in the standard release of CTH since version 8.0. For the simulations presented here the eos7860 tabular sesame was used, which was formulated for 4% moisture and bulk SiO_2 sand, where the grain density is 2.65 g/cc and the bulk density is 1.56 g/cc. The underlying reference curve for the construction of these tables was the shock Hugoniot for quartz measured by Wackerle [i]. Kerley suggested that the pore compaction pressure be approximate with:

$$P_s = (500\,MPa)e^{-19.2w}, \tag{1}$$

where w is the moisture content of the sand [xxii]. Thus assuming 4% moisture, we obtain a pore compaction pressure of 232 MPa, however it was found that a value of 1,440 MPa best fit the Hopkinson bar data. The bulk strength of the sand was modeled with a pressure dependent geological yield surface (GEO), previously implemented in CTH [xxiii]. The formulation for this yield surface is presented in Equation 2 and is illustrated in Fig. 2. Experimental data from buried land mine explosions suggest the yield-pressure correlation, dY/dP, is approximately 2 and would remain positive through compaction. The yield offset strength, Y', is approximately 80 MPa, and the bulk, zero pressure, yield

strength, Y_0, should be between 100-300 kPa, [xxi,xxii,xxiv]. The remaining material properties, obtained from a variety of sources [xxv-xxvii], are listed in Table 1. Note that variations in the bulk yield strength had little effect on the axial stress obtained given the loads far exceed these strengths.

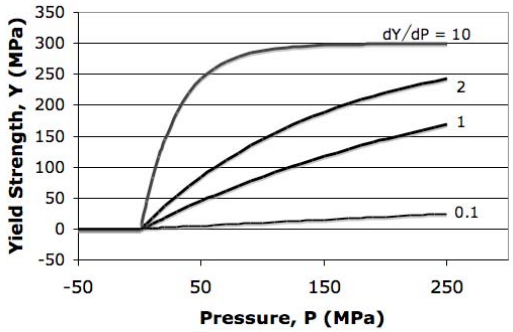

Figure 2: Pressure dependent geological yield surface

$$Y = Y' + (Y_0 - Y')\exp\left[\frac{P}{Y_0 - Y'}\frac{dY}{dP}\right] \quad \text{for } dY/dP > 0 \text{ and } P \geq 0$$

$$Y = \min\left\{Y', Y_0 + P\left|\frac{dY}{dP}\right|\right\} \quad \text{for } dY/dP < 0 \text{ and } P \geq 0$$

$$Y = Y_0 \quad \text{for } P<0 \qquad (2)$$

Table 1: Baseline constitutive relation constants for the continuum simulations

Tabular Equation of State Parameters[a]	Value	Pressure Dependent Geological Yield Parameters[a]	Value
Bulk Density, ρ_{00} [*g/cc*]	1.56	Max. Strength, Y' [MPa]	300
Grain Density, ρ [*g/cc*]	2.56	Yield Surface Slope, *dY/dP*	2
Pore compaction pressure, P_s [MPa]	232	Yield strength at zero pressure, Y_0 [MPa]	0.3
Zero stress shock speed, c_0 [*km/s*]	5.99	Poisson ratio, ν	0.32
Hugoniot slope, s	2.345	Tensile strength, σ_s [GPa]	0.0001

[a] Kerley [xxi,xxii]

Three-Dimensional Mesoscale Calculations

The computational domain and material properties utilized for the mesoscale simulations are presented in Fig. 3 and Table 2 respectively. Unlike the one-dimensional continuum simulations, a mesoscale approach resolves the grain interaction directly, thus there is no need to approximate the bulk material properties or include a pore compaction model.

A Mie-Grüneisen equation of state (EOS) [xxviii] with a perfectly elastic-plastic strength model was used to model each quartz sand grain. The EOS parameters are based on crystalline quartz, i.e. silicon dioxide (SiO_2); the main constituent of Ottawa sand is 99.8% pure quartz [xxix]. Quartz has famously demonstrated a rich variety of behaviors as a result of shock loading, including phase transitions, material property variability as a function of driving pressure and sample thickness, as well as stress relaxation effects. Given the nature of the Eulerian calculations, i.e. the inability to specify crystallographic orientation of individual sand grains as well as the polycrystalline nature of grains, different bulk material properties are assigned to each sand grain. For example, Table 2 list the shock Hugoniot properties of quartz as a function of the orientation of the crystalline structure [ii]. However, instead of assigning averaged properties to all of the grains, we explore the effect of assigning the x-cut shock Hugoniot properties to half of the grains in the simulation and z-cut properties to the other half.

The effect of varying the material properties is not new to this work; a more detailed exploration of theses effects can be found in Branson, Wells and Strack [xxx] and Borg [xxxi]. The specific heat of quartz is reported between 0.74 J/g/K and 0.85 J/g/K [xxxii,xxxiii].

For these simulations, the grains behave elastically until the specified dynamic strength is achieved, at which point the material plastically flows. Estimates of the Hugoniot elastic limit (HEL) for the x- and y-cut axes are between 5.5 GPa to 8.5 GPa and 10 to 15 GPa for the z-cut axis, however hydrostatic data indicate the lower limit is closer to 2.3 GPa [i,iii]. Simulations were conducted in which the HEL for all the grains was varied from 2 to 12.4 GPa. The measured Poisson's ratio for quartz varies between 0.11~0.15, however it was set to 0.15 for these simulations [i].

The measured dynamic tensile strength, i.e. spall strength, of quartz exhibits variations with respect to loading conditions. Kanel *et. al.* report that the spall strength for x-cut quartz reaches 4 GPa for loadings below the HEL and falls to zero for loading conditions near the HEL [xxxiv]. The dynamic tensile strength is extremely high as compared to the static fracture of 44 MPa [xxxv]. The loss in spall strength is thought to result from accumulated damage, i.e. cracking of brittle single crystals under compression, ultimately resulting in a total loss of tensile strength near the HEL. Much like the shock Hugoniot parameters, and in order to understand the effect of strength on the bulk compaction, a range of spall strengths were assigned to the grains within a given simulation. Simulations were carried out where the tensile strength was varied from pre-damaged or static fracture strengths, near zero, to 4 GPa.

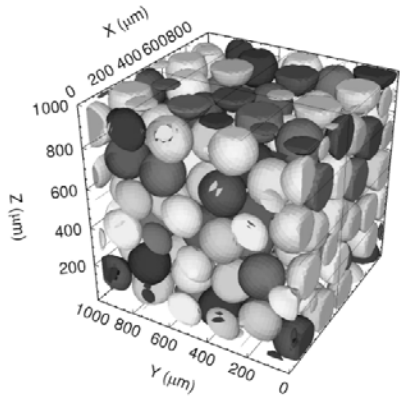

Figure 3: Three dimensional view of mesoscale geometry. Variations in gray scale are for visualization purposes only

Table 2: Baseline material and constitutive constants for the mesoscale simulations

Parameter	Quartz
Density, ρ [g/cm^3]	2.65
Zero stress shock speed, C_0 [*km/s*]	
x-cut	5.610
z-cut	6.329
Hugoniot slope, s	
x-cut	1.07
z-cut	1.56
Grüneisen coefficient, $\Gamma=V(\partial P/\partial E)_V$	0.9
Specific heat, C_V [*J/(g-K)*]	0.85
Bulk dynamic yield strength, Y [*GPa*]	
x-cut (low, average, high)	4.1, 5.8, 7.0
z-cut (low, average, high)	8.2, 10.3, 12.4
Poisson's ratio, ν	0.15
Fracture strength, σ_s [*GPa*	0.044 - 15 GPa

Given experimental observations that friction, be it grain-on-grain or between the sand and test fixture, has a significant effect on the resulting stress-strain behavior, we included some form of friction in the mesoscale simulation. Given the Eulerian nature of CTH, imposing a complete contact stress tensor on the surface of each grain would be difficult at best. However, CTH does allow the user to specify how the strength of a mixed material cells is calculated. When setting up the computational domains, care was taken to assign adjacent grains a different material number, thus enabling some control over the grain contact strength in mixed (i.e. touching) cells. We explored the effects of mixed cells being assigned either zero or the volume fraction averaged bulk yield strength: sliding or stiction

respectively. Sliding means there is no strength between materials in mixed cells, whereas stiction means that the initial grain network is welded. In either case, once the stress in a given cell exceeds the assigned strength, the material flows at the specified yield stress.

In previous high strain rate studies, 10^6 s^{-1}, conducted by the authors it has been found that mesh convergence is achieved for 10 computational cells per grain per spatial direction. In this study, where the strain rates are much lower, the mesh was such that 20 cells per grain were needed. Given these requirements and the three-dimensional nature of the domain, the simulations required approximately 100 hours utilizing 64 processors, whereas the one-dimensional simulations required 15 minutes utilizing a single processor. One can see the value of further developing continuum level simulations.

Results

Mesoscale Simulation Results

In order to explore the mesoscale results, the longitudinal stress, σ_{xx}, was averaged in the lateral direction for a given longitudinal position. The results are presented in Fig. 4 at two different snapshots in time, which translates to 19 and 31% strain, for both the stiction and sliding grain conditions. The simulations indicate that sliding results in substantially softer bulk stress as compared to stiction. A particular feature of these relatively slow strain rate events is that the stress state is fairly constant ahead of the incident bar (driver plate). The transmittal of information occurs at a rate, on the order of the sound speed of quartz (6, 000 m/s) or possibly as slow as the sound speed of bulk sand (~100 m/s), either of which is much faster than that of the driver plate (~1 m/s). In the context of a hydrocode written specifically to resolve wave phenomena this translates into hundreds of stress reverberations between the sample thickness. Thus as the driver plate compacts the sand at relatively constant velocity, a time varying (strain varying) stress-strain state is achieved within the sand.

These results provide a justification to average the entire stress state of the sand in order to obtain a bulk axial stress state for a given displacement, i.e. strain. The results, presented in Fig. 5, indicate that the sand with sliding grain contact requires very little applied stress to strain to nearly 25% as compared to the grains with stiction. The simulations indicate that the bulk compaction *snow plows* in its response, i.e. significant pore removal for little to no applied stress, before the bulk response stiffens. It is interesting to note that the maximum pack density of a monodisperse collection of spheres is $\pi/\sqrt{18}$ or 74%. Thus grain packing without friction slides together rather unimpeded until it is mechanically locks at near 25% strain, at which point the response stiffens. This behavior is illustrated in Fig. 5.

There are two modes in which grain material can be rearrange: 1) centroid motion, i.e. the grains moving without deforming and 2) grain deformation, i.e. a grain being deformed into a gap. For both the sliding and stiction simulations material is rearranged through a combination processes 1) and 2). The stiction simulations appear to have less centroid motion and more grain deformation as compared to the sliding simulation. The sliding simulations do not achieve a face centered cubic arrangement, i.e. maximum pack density. These assessments are purely qualitative; it is difficult to quantify how much of the material rearrangement is due to deformation and how much is due to centroid rearrangement.

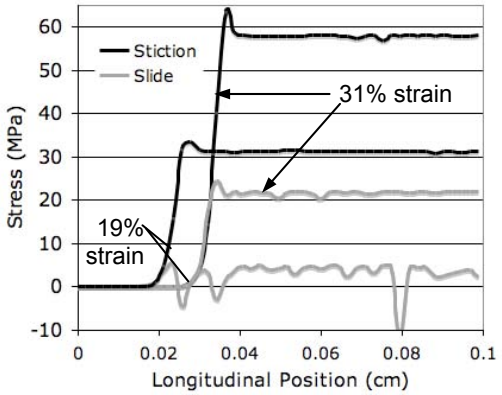

Figure 4: Average longitudinal stress for grains with either stiction or sliding at two different strains

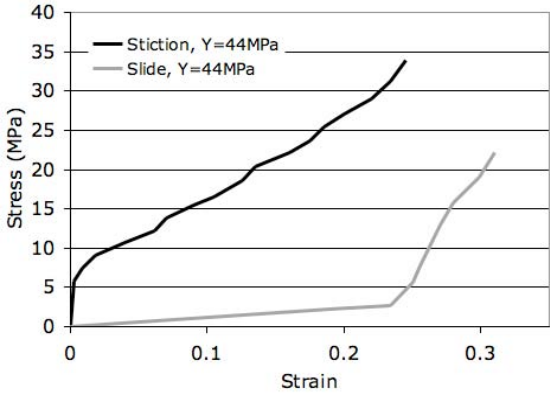

Figure 5 Stress-strain behavior for various grain and strength configurations

When compared to experimental stress-strain data, both the stiction and sliding grain conditions under predict the experimental behavior. Thus the average dynamic yield strength was increased by an order of magnitude, from 44 MPa to 440 MPa, to assess the effects on the bulk response; the results are presented in Fig. 6 along with experimental results for comparison. The results indicate an increase in the dynamic yield strength, over that of the static yield strength, is necessary to reproduce the experimental results. Since the sliding grain conditions indicated near snowplow like behavior, whereas the data did not, sliding simulations with higher yield strengths are not presented.

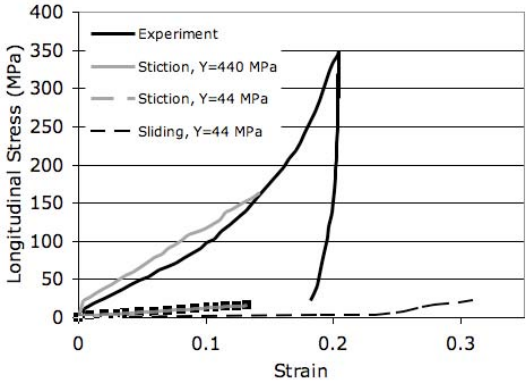

Figure 6: Bulk stress-strain for the mesoscale simulations as a function of grain boundary and dynamic yield strength

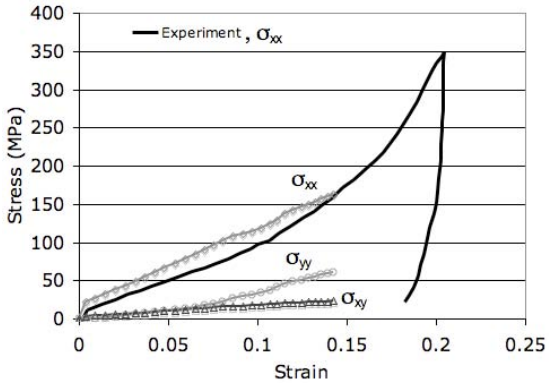

Figure 7: Stress tensor components for the mesoscale simulations with a dynamic yield strength of 440 MPa and stiction grain

In order to gain a better appreciation for the complete stress state achieved within the heterogeneous system both the averaged lateral stress and the averaged absolute value of the shear stress were computed from the mesoscale simulations and the results are presented in Fig. 7. Since the

average shear stress is zero; the absolute value of the shear stress was computed to gain an appreciation for amplitude of the relative shear compared to the longitudinal and lateral stress.

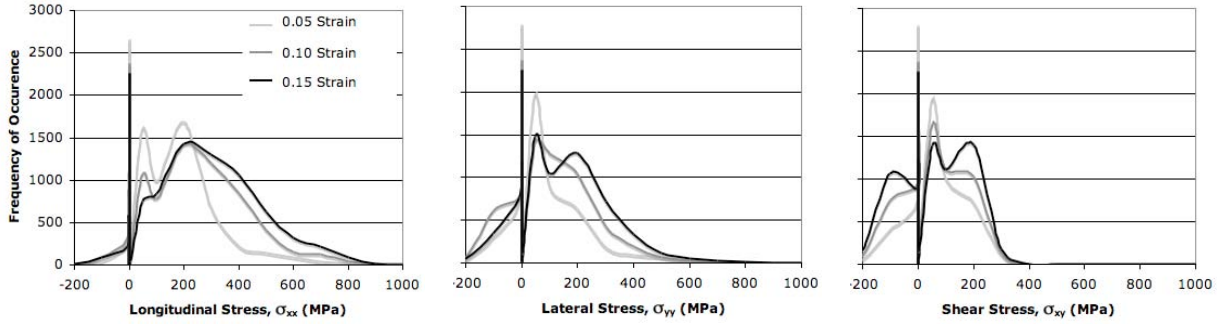

(a) (b) (c)

Figure 8: Stress distribution of averaged longitudinal, lateral and shear stress at 0.05, 0.1 and 0.15 strain

In order to better characterize the state of stress within the sand mixture, stress distributions were obtained from the mesoscale data. Figure 7 presents the distribution of the various tensor components of stress for all the computational cells within the simulation, at three different strains. The resulting distributions are non-normal (i.e. non-Gaussian). There are a large number of computational cells that experience no applied stress; these are represented as a large frequency of occurrence at zero. As a result, the most probable occurrence of stress, i.e. the average stress, does not appear centered on the distribution. For example, at 0.15 strain Fig. 7 indicates the average longitudinal stress, σ_{xx}, is approximately 160 MPa, which appears lower than the peak occurrence of stress presented in Fig. 8a for a strain of 0.15. In addition there are relatively high stress *hot spots* experienced within the sand which are not completely characterized by the average, i.e. some computational cells are experiencing stress nearly an order of magnitude higher than the average. Insights such as these, which are obtained from mesoscale simulations, could provide the way forward in our understanding of rapidly compacted heterogeneous systems, including both theoretical development and suggested experimental validation.

One-dimensional Simulation Results

Figure 9 presents the stress strain results from the one-dimensional simulations described above. Like the three-dimensional simulations, the one-dimensional simulations with the original parameters under predict the dynamic response of the sand. By increasing the stress at which all of the pores are removed (i.e. the stress at which the P-α curve intersects the quartz Hugoniot) from 440 MPa to 1440 MPa, the simulations more accurately follow the experimentally measured material response. This modification of the baseline one-dimensional material parameters is not in complete agreement with the three-dimensional mesoscale simulations. In the mesoscale simulations the complete removal of porosity corresponds to the intersection of the bulk dynamic response and the underlying material Hugoniot, which is near the dynamic strength assigned to the underlying material, i.e. 440 MPa. Thus the one-dimensional simulations require additional considerations.

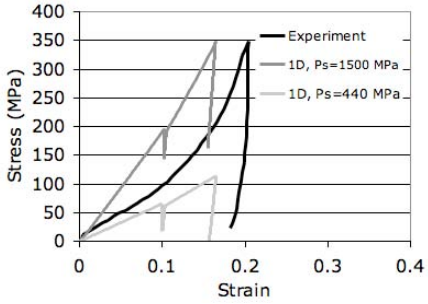

Figure 9: Bulk stress-strain curve for the continuum simulations yield strength with varying pore compaction strength

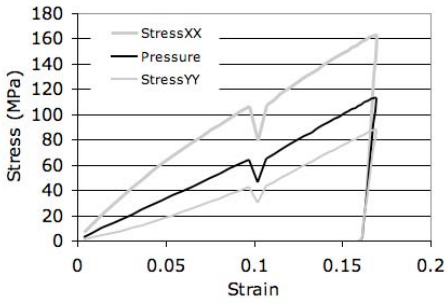

Figure 10: Stress tensor components for the continuum simulations with a pore compaction strength of 1500 MPa

Discussion

One unanticipated aspect of this work was the higher resolution required to converge the simulation, which is nearly twice that of previous higher strain rate mesoscale simulations [xii]. In general it is accepted that resolving each grain with 10 computational cells per grain, per axial direction is sufficient. However these lower strain rate simulations demonstrated significant variations in response up to 20 cells per grain per axial direction. This could be a result of the high number of iterations required to run the simulation out to nearly 6 ms and the advection problems associated with the large number of iteration performed in Eulerian simulations.

For the simulations presented here, a distribution of yield and fracture strength was applied to the grain network in order to access the effect on the bulk response. When applying a distribution of strength the key consideration is the average value. For the loading configurations investigated here, and the distribution of yield strengths from, 2 to 12.5 GPa, it was found that if the average did not vary then the bulk response did not vary. This is not the case for higher strain rate investigations, 10^6 s^{-1} [xxxi]. In the higher strain rate studies it was found that an underlying skeletal network of higher strength grains can form a percolated stress bridge which can stiffen the bulk response, this is especially true for stress levels near full compaction. For the lower strain rate studies conducted here, no such phenomena occurred. We are not sure if this is due to the allowable time for rearrangement, the low stress levels induced or the relatively narrow range of yield strength prescribed. Simulations presented here were sensitive to the variations in fracture strength, however. Varying the distribution of fracture strength could alter the bulk response of the grain network, even though the average value remained the same. This is especially true if one applies a dramatic distribution of fracture strengths, i.e. half the grains having a fracture strength of zero and half the grains having a fracture strength near the HEL. These results require further investigation.

The data presented in Fig. 7 is re-plotted in Fig. 11 along with two-dimensional mesoscale results from high strain rate simulations and accompanying experiments, shown as open circles and dashed lines respectively [x,xxxvi]. It is interesting to note that at higher strain rates, 10^6 s^{-1}, the presence of stiction over predicts the stiffness of the response as compared to experimental data [x,xxxvi]. It is important to keep in mind that the high strain rate experimental data was obtained from a one-dimensional flyer plate experiment, whereas the data presented above was obtained from a Hopkinson

bar. The mesoscale simulations are nearly identical except they are at higher incident bar velocities and two-dimensional.

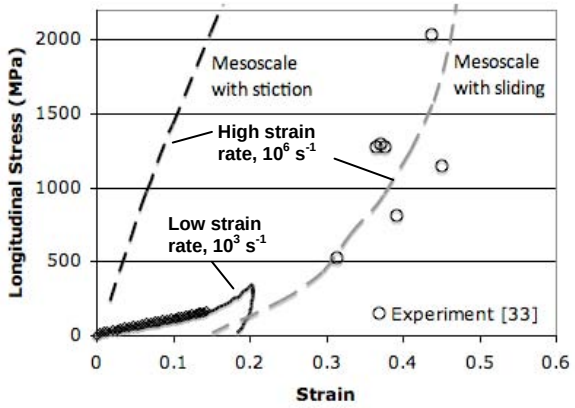

Figure 11: A comparison of high, 106 s-1, and low, 103 s-1, strain rate data and simulation. Low strain rate data from Fig. 7. High strain rate data, open circles, and accompanying mesoscale simulations, dashed lines, with stiction or sliding [10,36]

As Fig. 11 indicates, the sliding boundary condition better represents the experimentally determined dynamic response of the material at higher strain rate. Both high and low strain rate simulations suggest that grain contact interactions can have a significant effect on the bulk response of the heterogeneous material but that the relevant contribution of friction varies as the strain rate varies, i.e. friction is important at low strain rates, with dimensioning importance at higher strain rates. Exploring these effects will continue for future studies.

Conclusions

Mesoscale simulations, such as those presented here, provide a rich backdrop for the exploration of rapidly compacted heterogeneous systems. Mesoscale simulations, which are a fairly new idea within the computational community, have yet to realize their full potential as a research tool in conjunction with experimental techniques, theoretical development and/or continuum simulations. The simulations presented here indicate that low strain rate Eulerian mesoscale simulations require fairly high resolution to accurately predict the averaged longitudinal stress of a dynamically compacted sand sample. In addition, the simulations required that the dynamic strength be an order of magnitude higher than the static yield strength. The simulations further indicate that the presence of stiction (friction) is necessary to accurately predict the stress-strain behavior as compared to experimental data. From the simulations a complete description of the averaged stress state, the longitudinal, lateral and shear stress, can be obtained. In addition, the simulations also indicate that this stress state is non-normal distributed within the sand sample and hot spots of stress can exists which are nearly ten times that of the average axial stress measured by the experiment.

Acknowledgements

This work was co mpleted with fundin g support provided by the Air Force Research Laboratory under contract F1TBAX9111B701.

References

[i] Wackerle, J. *J. Appl. Phys*., 33 (3), 922-937. 1962.
[ii] Anan'in, AV, Breusov, ON, Dremin, AN, Persh in, SV and Tatsii, VF. *Combust. Explo. Shock*, 10 (3), (1974), 372-379.
[iii] Fowles, R., *J. Geophys. Res.*, 72(22) (1967), 5729.
[iv] Turin, RF. Shock Compression of Condensed Materials, Cambridge Press , 1998.
[v] Carroll, M.M and Holt, A.C, Static and dynamic pore-collapse relations for ductile porous materials. Journal of Applied Physics. 43 1626-1636, 1972
[vi] Asay, J.R. and Shahinpoor M., *High-Pressure Shock Compression of Solids*, Springer-Verlag, 1993, pg 7
[vii] Hermann, W. Constitutive equation for the dynamic compaction of ductile porous materials, Journal of Applied Physics, 40 (6) , 2490-2499, 1969
[viii] Grady D.E. and Winfree N.A. (2001). A computational model for polyurethane foam, In K. P. Staudhammer, L.E. Murr, and M.A. Meyers, editors, *Fundamental issues and applications of shock-wave and high-strain-rate phenomena, Proceedings of EXPLOMET*, pages 485–491.
[ix] Wunnemann K., Collins G.S., Melosh H.J. Icarus 180, 514-527, 2006
[x] Borg, J.P. and Vogler, T.J., The Effect of Water Content on the Shock Compaction of Sand in Proceedings of the Dynamic Behavior of Materials, DYMAT 2009 Brussels Belgium, pg 1545–1551
[xi] Crawford, D.A. 2005. Using mesoscale modeling to investigate the role of material heterogeneity in geologic and planetary materials. In: Shock compression of Condensed Matter – 2005, pp. 1453-1457.
[xii] Borg, J.P. and Vogler, T .J., Mesoscale calculations of the dynam ic behavior of a gra nular ceramic *Int. J. Solids Struct.* 45, 1676–1696, 2008
[xiii] Benson, D.J., Nesteren ko, V.F., Jonsdottir, F.F. an d Meyers, M.A. Quasistatic and dynamic regimes of granular matrial deformation under impulse loading *J. Mech. Phys. Solids*, **45(**11) 1955-1999, 1997
[xiv] Nesterenko, V.F., *Dynamics of Heterogeneous Materials*. Springer, 2001
[xv] Tong, W, Ravichandran, F., Christman, T. and Vreeland T., 1995. Acta Materialia 43, 230-250.
[xvi] Martin, B.E., Chen, W., Song, B., Akers, S.A., "Moisture effects on the high strain-rate behavior of sand" Mechanics of Materials (in press)
[xvii] Martin, B.E., and Chen, W. "The High-Rate Behavior of a Fine Grain Sand" Proceedings of the SEM Annual Conference, June 1-4, 2009 Albuquerque New Mexico USA
[xviii] Martin, B.E., and Chen, W. "Response of Moist Sand to High Rate Loading" Proceedings of the DYMAT 2009, EDP Sciences, 201–205, 2009, Brussels Belgium
[xix] Bragov, AM, Kotov, VL, Lomunov, AK, and Sergeichev, IV, "Measurement of the Dynamic Characteristics of Soft Soils Using the Kolsky Method". J. Appl. Mech. Tech. Phys., 45(4), 580-585, 2004
[xx] McGlaun, J. M. Thompson, S. L. and Elrick, M. G., "CTH: a T hree-Dimensional Shock Wave Physics Code," *Int. J. Impact Engng.*, **10**, 351-360, 1990.
[xxi] Kerley, GI, The Effects of Soil Type on Numerical Simulations of Buried Mine Explosions, Kerley Technical Services report KTS02-3, August 2002.
[xxii] Kerley, G.I., On the Numerical Simulation of Buried Mine Explosions: Choosing Constitutive Models. Kerley Technical Services, KTS05-3, Aug. 2005

[xxiii] Crawford, DA, Bell, RL, Brundage, AL, Bruner, CW, Elrick, MG, Hertel, ES, Schmitt, RG, Schumacher, SC, Silling, SA, Simmons JS and Taylor, PA. CTH User's Manual and Input Instructions Version 8.1, Nov. 2007

[xxiv] Windham, J., U. S. Army Engineer Research and Development Center, Waterways Experiment Station, Vicksburg, MS, private communication.

[xxv] Velea, D. S hields, FD a nd Sabatier JM. "Elastic wave velocities in partially satu rated Ottawa sand: experimental results and modeling" *Soil Sci. Soc. Am. J.* 64, 1226–1234, 2000.

[xxvi] Verma, DK and Shaw, DS. "A comparison of international silica (α-quartz) calibration standards by fourier transform–infrared spectrophotometry" *Ann. Occup. Hyg.*, 45(6), 429–435, 2001.

[xxvii] Hertel, ES and Kerley, GI. "CTH EOS package: introductory tutorial", Sandia Report 98-0945, 1998.

[xxviii] Rice, MH, McQueen, R.G. and Walsh, J.M. "Compression of Solids by Strong Shock Waves" *Solid State Phys*. 6 (1), 1958.

[xxix] American Society for Testing and Materials (ASTM) standard C-778

[xxx] Brannon, R. M., Wells, J., M., Strack, O.E., "Validating theories for brittle damage," Metallurgical and Materials Transactions A 38A, 2861-2868, 2007.

[xxxi] Borg, JP and Vogler, TJ, "The Effect of Water Content on the Shock Compaction of Sand", in DYMAT 2009 - 9th International Conferences on the Mechanical and Physical Behaviour of Materials under Dynamic Loading, vol. , 2009, pp. , 1545-1552, published by EDP Sciences (www.dymat-proceedings.org).

[xxxii] Grady, D.E. *J. of Geophysical Research* 85, N. B2, (1980), 913-924.

[xxxiii] Schroeder, DV., An Introduction to Thermal Physics, Addison-Wesley, 2000.

[xxxiv] Kanel', Razorenov and Utkin, *High-Pressure Shock Compression of Solids II* edited by Davison, Grandy and Shahinpor, Springer (2004) pg 121

[xxxv] C.H. Scholz, *J. of Geophysical Research*, 77 (11), 1972

[xxxvi] Chapman, DJ, Tsembelis, K, Proud WG Proceedings of the 2006 SEM annual conference and exposition St. Louis, MO June 4-7 2006

DISTRIBUTION LIST
AFRL-RW-EG-TR-2011-052

Defense Technical Information Center — 1 Electronic Copy (1 File & 1 Format)
Attn: Acquisition (OCA)
8725 John J. Kingman Road, Ste 0944
Ft Belvoir, VA 22060-6218

EGLIN AFB OFFICES:

AFRL/RWOC (STINFO Office)- 1 Hard (Color) Copy
AFRL/RW CA-N - STINFO Officer Provides Notice of Publication
AFRL/RWME - 1 Copy
AFRL/RWMF - 1 Copy
AFRL/RWMW - 1 Copy
AFRL/RWMI - 1 Copy